FLIGHT DYNAMICS ISSUES RELATING TO AUTOGYRO AIRWORTHINESS AND FLIGHT SAFETY*

Vassilios M. Spathopoulos
Dr Stewart S. Houston
Dr Douglas G. Thomson

Department of Aerospace Engineering
University of Glasgow
Glasgow G12 8QQ U.K.

Abstract

This paper presents an analysis of flight test and simulation data obtained from two gyroplanes. This class of rotary-wing aircraft has found limited application in areas other than recreational flying, however, the accident rate is such that a study of the configuration's stability and control characteristics is timely. The longitudinal stability characteristics of two gyroplanes are presented thus helping to consolidate the understanding of this type of aircraft by means of documenting its attributes. It is concluded that unusually for rotorcraft in general, the type examined displays "classical" longitudinal dynamic stability characteristics, with the rotorspeed degree of freedom being of vital importance. Interpretation of the identified stability derivatives indicates that the vertical position of the centre of mass in relation to the propeller thrust line may have an important role to play in gyroplane longitudinal stability. The results contribute directly to the development of the UK gyroplane airworthiness and design standard, BCAR Section T in the important areas of dynamic stability, and weight and balance.

Nomenclature

M_u, M_w, etc.	pitching moment derivatives, 1/ms
p,q,r	angular velocity components about body axes, rad/s
R	regression correlation coefficient
T, T_p	rotor, propeller thrust, N
$T(u, w)$	rotor thrust in (u, w) disturbed flight, N
T_u, T_w, etc	rotor torque derivatives, rev/min/m
u, v, w	velocity components along longitudinal, vertical body axes, m/s
u_{probe}, w_{probe}	velocity components along longitudinal, vertical air data probe axes, m/s
X_u, X_w, etc	longitudinal body axis acceleration derivatives, s^{-1}
$\underline{x}, \underline{u}$	state and control vectors
$\underline{x}(\omega), \underline{u}(\omega)$	Fourier-transformed state and control vectors
$x_{vane}, y_{vane}, z_{vane}$	angle of attack and sideslip vane location in body axes, m
x_{cg}, y_{cg}, z_{cg}	aircraft centre-of-mass position in body axes, m
Z_u, Z_w, etc	vertical body axis acceleration derivatives, s^{-1}
$\alpha_{vane}, \beta_{vane}$	angle of attack and sideslip measured at vane location, rad
Δf	frequency increment, rad/s
Δt	time increment, s
δ_p	propeller speed, rad/s
δ_r	rudder position, % (0% fully right)
η_c	lateral stick position, % (0% fully left)
η_s	longitudinal stick position, % (0% fully forward)
ϕ, θ, ψ	aircraft attitudes, rad
Ω	rotorspeed, rev/min

* Presented at the American Helicopter Society 54th Annual Forum, Washington, DC, May 20-22, 1998.

Introduction

There are a wide range of configurations in the class of aircraft known as rotorcraft. The helicopter is the most common type, finding widespread application in commercial and military aviation. The gyroplane (or autogyro), however, is an increasingly popular machine in sport and recreational flying, having found no practical application in contemporary commercial or military roles.

Currently, most if not all types of this aircraft are in the homebuilt, or experimental category. The study of the configuration's flight mechanics is timely, given the accident rate suffered by the aircraft. For example, Ref. 1 states that between 1989-1991, the autogyro fatal accident rate in the U.K. was 6 per 1000 flying hours, whereas the overall general aviation rate during 1990 was 0.015 per 1000 flying hours. As a consequence there is a heightened interest in this class of aircraft, and a new airworthiness and design standard (BCAR Section T) has been published by the U.K. Civil Aviation Authority, Ref. 2.

The gyroplane helped to pave the way for the development of the helicopter, introducing cyclic pitch control and blades attached to the rotor hub by means of a hinge. Unfortunately, with the one exception of Ref. 3, the literature has not hitherto addressed stability and control. The literature on gyroplanes nonetheless is considerable, Refs. 4-14 for example. In a contemporary context, this work is now primarily of historical significance. It provides the basis of the understanding of gyroplane flight, but does not address the issues of stability and control. Examination of the literature shows a logical development of the study of gyroplanes, from the elementary theory of gyroplane flight, to an analysis of aerodynamics and performance and ultimately rotor behaviour, but only for steady flight. Interest then apparently waned and the next logical stage in the study of the gyroplane i.e. stability and control, was not examined. For example, the work of Glauert includes the derivation of simple expressions for rotorspeed as a function of loading and axial velocity, Ref. 4. Wheatley, Ref. 10 derived expressions for the flapping angles required for equilibrium flight, presenting results that show how coning, longitudinal and lateral flap angles vary with flight condition. These analyses would be recognisable today as classical rotary-wing theory and analogous to that found in helicopter text books. Wheatley even examined higher harmonic components of blade flapping behaviour, Ref. 12.

It is in this context that flight trials and the associated data analysis methods were planned for the VPM gyroplane and are being prepared for the Montgomerie Glasgow University research autogyro. The analysis performed for the VPM aircraft was part of a contract between the University and the Civil Aviation Authority. The aircraft is presented in **Figure 1.**

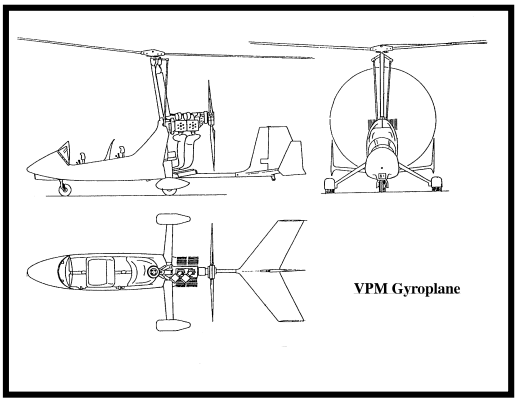

Figure 1: The VPM gyroplane

The stability characteristics were extracted using a frequency-domain equation-error method using linear regression, to synthesise conventional 3 degree-of-freedom stability and control derivatives. The results were then used to validate a sophisticated blade element/individual blade simulation model developed from the Department's substantial experience in rotorcraft modeling (Ref. 15). This model was then used to predict the performance of the Montgomerie gyroplane, which is illustrated in **Figure 2**.

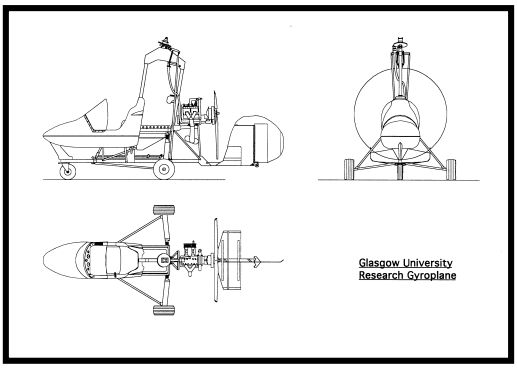

Figure 2: The Montgomerie gyroplane

The aircraft is due to be flight tested during the summer of 1998 with the specific objectives of deriving its stability and control characteristics and expanding the database of knowledge of this class of aircraft.

The objective of this paper is to consolidate the understanding of this type of aircraft by documenting characteristics of different types, with a view to creating a data base of characteristics. The information derived can then be used in the development of airworthiness and design standards. The specific aims of the paper are to review the results produced from the study of the VPM M16 autogyro; to repeat the study for the Montgomerie Glasgow University research autogyro; to catalogue and compare their attributes; and to use the results to assess the nature of flight dynamics of autogyros.

Aircraft Flight Testing

The aims of the flight test program were to investigate the stability and control characteristics of a type of aircraft for which little substantive data of this nature exists. The modes of motion were excited in the conventional way and the state time histories were used to extract the stability derivatives, thus providing good insight to the performance of the aircraft.

VPM Results

The VPM aircraft is of Italian origin and has a maximum all-up mass of 450 kg, see Appendix. The aircraft is powered by a four-cylinder two-stroke engine driving a three-bladed fixed pitch propeller. The experimental installation consisted of a digital on-board recording system, operating at 10 Hz. Anti-aliasing filters were incorporated. A nose-mounted air data probe containing sideslip and angle of attack vanes was fitted, and an inertial unit measured angular velocities about three axes, and linear accelerations along these axes. A separate unit was used to measure roll and pitch angles. Pilot control positions were measured using potentiometers. Rotorspeed was also recorded.

The 3 degree-of-freedom longitudinal model structure was used since it is familiar to flight dynamicists, thereby facilitating general insight into fundamental behaviour of the gyroplane. Specific derivatives are directly related to individual, or group, effects that would otherwise be hidden in the aggregate presentation of a frequency response. The equation error method has limitations, as described in Refs. 16 and 17, although working in the frequency domain minimises some of the difficulties. The advantage is the simplicity of the approach, in concept and application. It is argued that good results can be obtained with a frequency-domain equation-error approach if careful design of the experiments, the equipment installation and execution of the flight trials is complemented by sound engineering judgement applied to the interpretation of the data. The model structure for which coefficients are to be identified, is of conventional state-space form, i.e.

$$\dot{\underline{x}} = A\underline{x} + B\underline{u} \tag{1}$$

where

$$A = \begin{bmatrix} X_u & X_w & X_q & X_\theta & X_\Omega \\ Z_u & Z_w & Z_q & Z_\theta & Z_\Omega \\ M_u & M_w & M_q & M_\theta & M_\Omega \\ 0 & 0 & 1 & 0 & 0 \\ T_u & T_w & T_q & T_\theta & T_\Omega \end{bmatrix}, B = \begin{bmatrix} X_{\eta_s} \\ Z_{\eta_s} \\ M_{\eta_s} \\ 0 \\ T_{\eta_s} \end{bmatrix} \tag{2}$$

and

$$\underline{x} = [u\ w\ q\ \theta\ \Omega]^T, \underline{u} = [\eta_s] \tag{3}$$

This constitutes the longitudinal subset of the conventional 6 degree-of-freedom rigid-body flight mechanics model, with the important addition of the rotorspeed degree of freedom. The rigid body states are taken to be with respect to a mutually orthogonal, right-handed frame of reference whose origin is at the centre of mass. The longitudinal and vertical axes are respectively parallel and normal to the keel of the aircraft.

The angular quantities in the state vector, and the control position, are all measured directly. The translational velocities u and w are obtained from airspeed, sideslip and angle of attack data measured at the nose-mounted boom, as follows.

$$\begin{aligned} u &= u_{probe} - q(z_{vane} - z_{cg}) + r(y_{vane} - y_{cg}) \\ w &= w_{probe} - p(y_{vane} - y_{cg}) + q(x_{vane} - x_{cg}) \end{aligned} \tag{4}$$

and

$$u_{probe} = \frac{V_f \cos\beta_{vane}}{\sqrt{1+\tan^2\alpha_{vane}}};\ w_{probe} = u_{probe}\tan\alpha_{probe} \tag{5}$$

The time histories of each variable were then converted into frequency domain information using a Discrete Fourier Transform, Ref. 18, given by

$$X(k\Delta f) = \Delta t \sum_{n=0}^{N-1} x_n e^{-i2\pi(kn)/N};\ k = 0,1,2,...,N-1 \qquad (6)$$

which gives real and imaginary parts of X ,

$$\begin{aligned} \mathrm{Re}[X(k\Delta f)] &= \Delta t \sum_{n=0}^{N-1} x_n \cos(2\pi(kn)/N); \\ \mathrm{Im}[X(k\Delta f)] &= -\Delta t \sum_{n=0}^{N-1} x_n \sin(2\pi(kn)/N) \end{aligned} \qquad (7)$$

The quality of these frequency domain data can be enhanced by standard processing techniques such as applying overlapped and tapered windows to the data, as recommended by Tischler, Ref. 18.

Each degree of freedom can then be treated separately, and formulation as a linear regression problem allows estimation of the coefficients. The state-space description is converted to the frequency domain, i.e.

$$i\omega \underline{x}(\omega) = A\underline{x}(\omega) + B\underline{u}(\omega) \qquad (8)$$

Note that this assumes that any process noise is zero. The unknown coefficients of the A and B matrices are determined by solutions of the frequency domain equations

$$\begin{aligned} -\omega\,\mathrm{Im}[\underline{x}(\omega)] &= A(\mathrm{Re}[\underline{x}(\omega)]) + B(\mathrm{Re}[\underline{u}(\omega)]) \\ \omega\,\mathrm{Re}[\underline{x}(\omega)] &= A(\mathrm{Im}[\underline{x}(\omega)]) + B(\mathrm{Im}[\underline{u}(\omega)]) \end{aligned} \qquad (9)$$

This solution applies equal weighting to real and imaginary part errors, which is consistent with the standard weighting for system identification on a Bode plot. The pitching moment equation for example, is then expressed as the two equations

$$\begin{aligned} -\omega\,\mathrm{Im}[q(\omega)] &= M_u\,\mathrm{Re}[u(\omega)] + M_w\,\mathrm{Re}[w(\omega)] \\ &+ M_q\,\mathrm{Re}[q(\omega)] + M_\theta\,\mathrm{Re}[\theta(\omega)] \\ &+ M_\Omega\,\mathrm{Re}[\Omega(\omega)] + M_{\eta_s}\,\mathrm{Re}[\eta_s(\omega)] \end{aligned} \qquad (10)$$

$$\begin{aligned} \omega\,\mathrm{Re}[q(\omega)] &= M_u\,\mathrm{Im}[u(\omega)] + M_w\,\mathrm{Im}[w(\omega)] \\ &+ M_q\,\mathrm{Im}[q(\omega)] + M_\theta\,\mathrm{Im}[\theta(\omega)] \\ &+ M_\Omega\,\mathrm{Im}[\Omega(\omega)] + M_{\eta_s}\,\mathrm{Im}[\eta_s(\omega)] \end{aligned}$$

The other degrees of freedom are in a similar form.

The test points were nominal airspeeds of 30, 50 and 70 mph. At each of these speeds, a doublet-type input was used to excite the short-term response, and the standard technique of displacing the stick to provoke a speed change before returning it to trim was used to excite any phugoid. Frequency sweep inputs were conducted only at the 70 mph test point. **Figure 3** illustrates a typical frequency sweep.

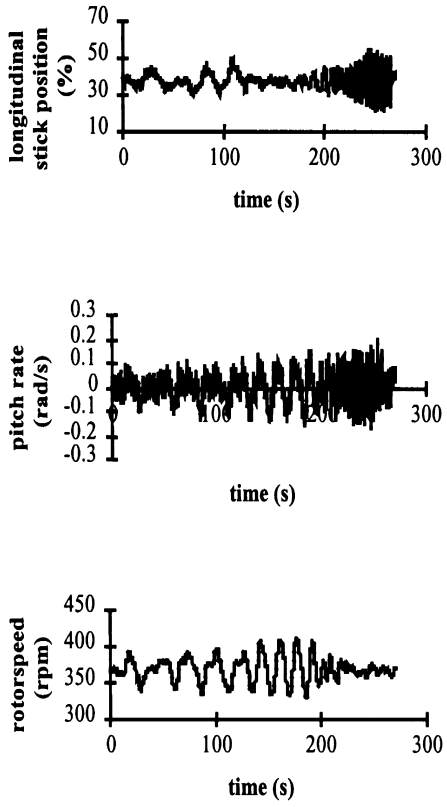

Figure 3: Response during frequency sweep test at 70 mph

Data from doublet and phugoid tests were zero-meaned and concatenated to provide a 90 second record length. The longitudinal derivatives estimated using these data are compared in **Table 1**, with derivatives estimated from a frequency sweep. The standard error associated with each derivative is given in parentheses.

Consistent estimates of the derivatives are obtained, particularly in the pitching moment and rotor torque equations and the correlation

coefficients are also good, in general. The standard error associated with each estimate is relatively small, although for frequency sweep-derived parameters the errors are generally smaller than with the concatenated doublet/phugoid. Although the force derivative estimates display less consistency than the pitching moment and rotor torque estimates, this is consistent with parameter estimation experience in general, where force derivatives have been more difficult to identify than moment derivatives. However, it is argued that these force derivative estimates are consistent to within the statistical error bounds associated with each derivative.

parameter	concatenated doublet/phugoid	frequency sweep
R	0.742	0.822
X_u	0.081 (0.056)	0.047 (0.025)
X_w	-0.126 (0.109)	-0.268 (0.058)
X_q	-3.976 (3.499)	-1.169 (1.380)
X_θ	-9.036 (1.578)	-10.632 (0.851)
X_Ω	-0.044 (0.013)	-0.025 (0.006)
X_s	0.010 (0.034)	-0.001 (0.013)

a. X-force Derivatives

parameter	concatenated doublet/phugoid	frequency sweep
R	0.919	0.886
M_u	0.023 (0.003)	0.021 (0.001)
M_w	-0.065 (0.007)	-0.064 (0.003)
M_q	-1.213 (0.126)	-1.055 (0.076)
M_θ	-0.449 (0.181)	-0.294 (0.047)
M_Ω	-0.001 (0.0006)	-0.001 (0.0003)
M_{η_s}	0.029 (0.001)	0.028 (0.0007)

b. Pitching Moment Derivatives

parameter	concatenated doublet/phugoid	frequency sweep
R	0.928	0.706
Z_u	-0.060 (0.025)	-0.128 (0.024)
Z_w	-0.788 (0.048)	-0.565 (0.057)
Z_q	23.665 (1.529)	26.446 (1.350)
Z_θ	2.247 (0.690)	4.060 (0.832)
Z_Ω	-0.054 (0.005)	-0.065 (0.006)
Z_{η_s}	-0.100 (0.015)	-0.098 (0.013)

c. Z-force Derivatives

parameter	concatenated doublet/phugoid	frequency sweep
R	0.910	0.966
T_u	1.373 (0.166)	1.378 (0.042)
T_w	5.324 (0.628)	5.901 (0.126)
T_q	12.590 (12.419)	7.679 (3.076)
T_θ	0 - fixed	0 - fixed
T_Ω	-0.129 (0.029)	-0.085 (0.007)
T_{η_s}	0.305 (0.129)	0.314 (0.030)

d. Rotorspeed Derivatives

Table 1: Derivative comparisons

The standard errors indicate that the corresponding derivatives will lie within the 95% confidence bounds associated with their respective estimates.

Derivatives that physically ought to have negligible aerodynamic or propulsion force and moment contributions (i.e. those dominated by kinematic or gravitational terms), are X_θ and Z_q. The former ought to have a value of approximately -9.81. Both input types give estimates of X_θ and Z_q that are very similar, and in the case of Z_q also consistent with the mean flight speed of 28 m/s. This enhances confidence in the frequency sweep-derived Z-force derivatives, despite this equation providing the lowest correlation coefficient. Note that terms normally expected to be negligible or zero, such as Z_θ and M_θ, were retained in the regression as an additional check on model structure validity.

The derivative Z_θ is not negligible, although it is estimated with a relatively large standard error, and removing it from the regression proved to have little impact on the quality of fit or the other parameters in the model. Removing M_θ from the pitching moment model also had little effect on the other estimates, although it is estimated with a relatively low standard error, tending to suggest that it should be retained. However, its contribution to the overall pitching moment is approximately an order of magnitude smaller than the other terms in the equation, for the perturbations in $\underline{x}$ and $\underline{u}$ experienced in flight.

Estimates for the X-force derivative X_u are very small, with relatively large standard error. Indeed, the frequency sweep-derived value is positive. This parameter is the primary damping term in the phugoid mode, Ref. 19, and it would normally be expected to be substantially negative. As will be seen later in this paper, inspection of the airspeed time histories suggests consistency with the identified values of X_u, in that there is little apparent damping of airspeed during the longer-term, phugoid-type oscillation.

The pitching moment derivatives M_u, M_w and M_q describe an aircraft with classical longitudinal stability characteristics. Speed stability is positive ($M_u > 0$), angle of attack stability is positive ($M_w < 0$) and the primary pitch damping is positive ($M_q < 0$).

Montgomerie Experimental Set-Up

Lessons learned in the CAA trails have been put into practise in the design of the sensor and data acquisition packages for the in-house aircraft. Data acquisition is by a Kontorn Elektronik industrial PC recording 64 channels at a sample rate of 64Hz using a National Instruments DAQ card and Labview software, telemetry being possible via a radio modem link. Initial trails will focus on recording standard flight dynamics data and hence the sensor package consists of:

i) one British Aerospace Systems and Equipment three axis accelerometer to measure the component inertial accelerations,
ii) three British Aerospace Systems and Equipment rate gyros to measure the attitude rates,
iii) three British Aerospace Systems and Equipment angle indicators to measure attitude angles,
iv) one Space Age Technology mini air data boom to measure airspeed, angle of attack and angle of sideslip,
v) four Space Age Technology displacement transducers to measure the pilot's control inputs (fore and aft stick, pedals and throttle).

The aircraft is equipped with a Garmin GPS receiver, the data from which will also be downloaded to the on-board computer. A baseline set of flight trials to ascertain the basic performance, and stability and control characteristics of the aircraft is being planned for the summer of 1998. Subsequent trials will be performed to support the current rotorcraft research in the Department, for example strain gauges and pressure transducers will be fitted to the blades to validate current modelling projects in the areas of wake dynamics and blade aeroelasticity.

Model Validation

The mathematical model used for simulating the gyroplane performance is described in detail in Ref. 15 and is the product of several years of development within the Department. Data from the appropriate flights was used to compare with the trim results and to those regarding the stability and control derivatives, for the model minimum and maximum weights.

Comparison of Trim Results

Figure 4 shows the comparisons in pitch and roll attitude. The result shown for the roll, illustrate an excellent correlation between flight and model. The

pitch attitude predictions tend to indicate that the trend with speed is more accentuated with the model. Extensive numerical experiments have been conducted with the model, but this has failed to give any substantive reason for the discrepancy. This mismatch is only below 35 mph. This error can be placed in some context by considering that, in piloting terms, one can obtain information from an artificial horizon only to a resolution of 2.5 deg.

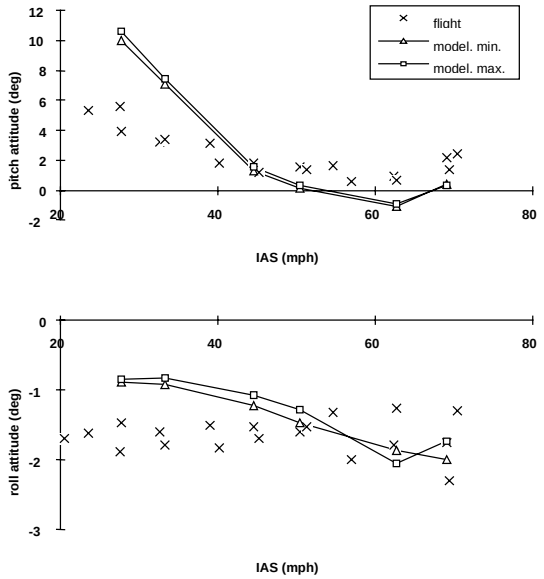

Figure 4: Roll and pitch attitudes from model and flight test

Figure 5 shows the control angles required to trim. Lateral and longitudinal stick position with speed is accurately matched by the model. This is particularly important in the case of longitudinal stick position, as it shows that the model accurately mimics an important handling qualities parameter, that of speed static stability.

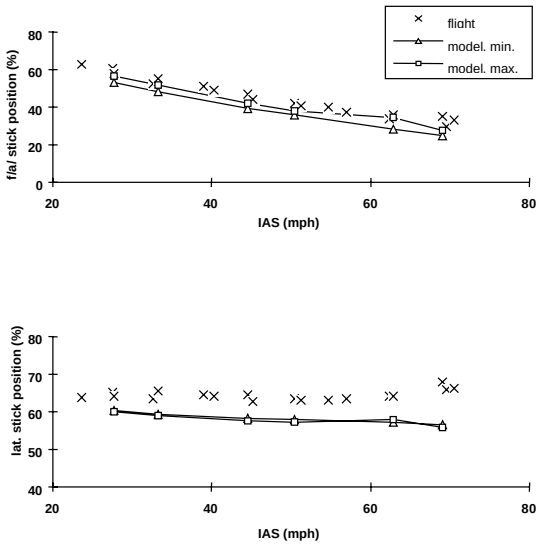

Figure 5: Control angles from model and flight test

Finally, **Figure 6** compares flight and model rotorspeed. Trend with speed is consistent although there is a slight mismatch across the speed range. This is nonetheless a significant result, given that the rotor is not driven by shaft torque and governed to a particular value as it would be in the helicopter simulation.

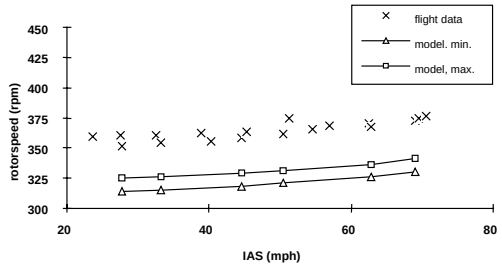

Figure 6: Rotorspeed from model and flight test

Comparison of Stability and Control Derivatives

The simulation model is of an individual blade/blade element type. The equations of motion are therefore periodic, and hence difficult to interpret. Linearising the model in the conventional 6 Degree-of-Freedom (DOF) form familiar to stability and control engineers, is possible.

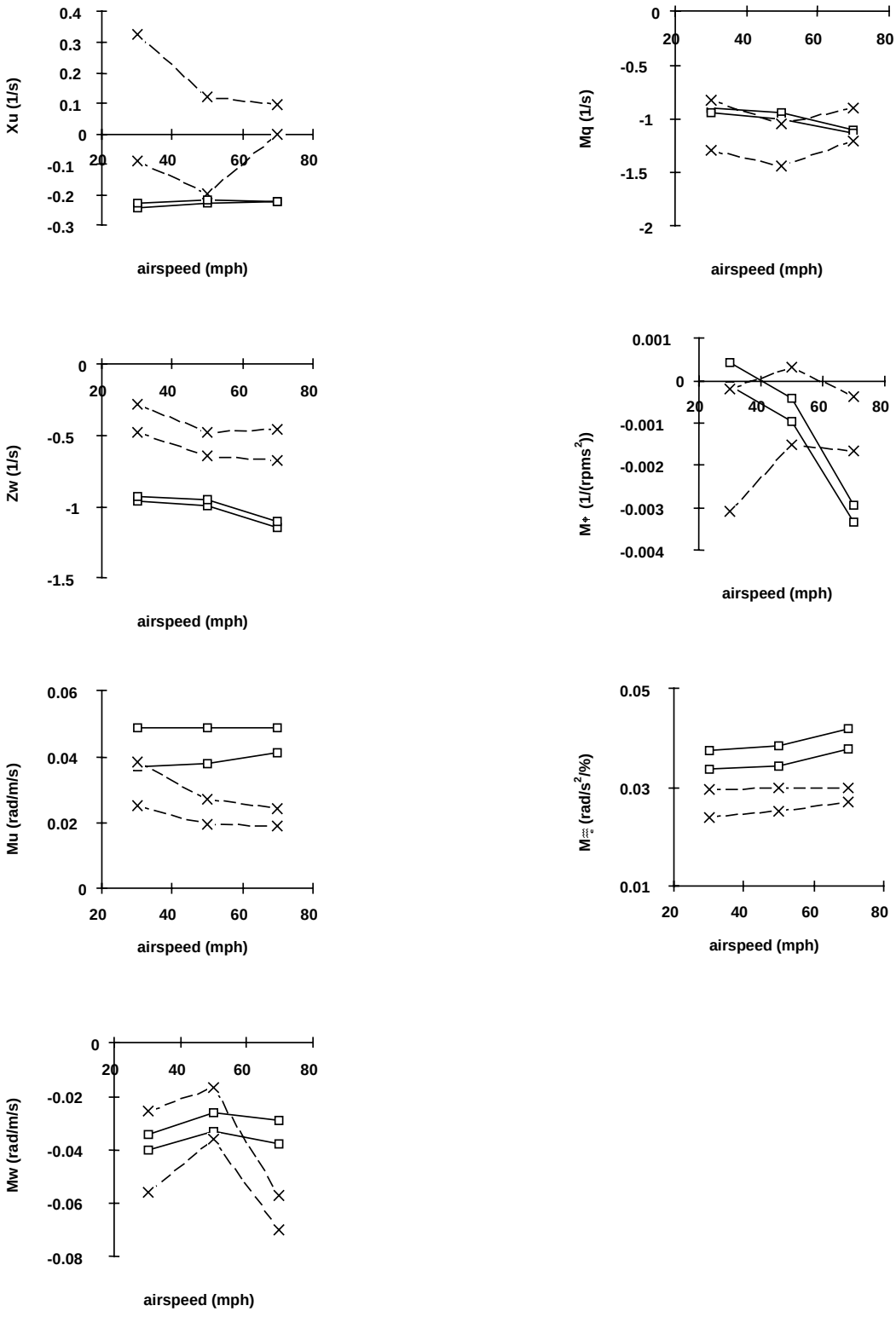

Figure 7: Key longitudinal derivatives

The model is then of the form

$$\dot{\underline{x}} = A\underline{x} + B\underline{u}$$

Where,

$$\underline{x} = [u\ v\ w\ p\ q\ r\ \phi\ \theta\ \psi]^T \text{ and } \underline{u} = [\delta_r\ \eta_s\ \eta_c\ \ \delta_p]^T$$

The coefficients in the matrix A are the conventional stability derivatives, those in B the control derivatives.

Figure 7 presents the 95% confidence, 95% probability bounds of those identified derivatives that tend to determine fundamentally the dynamic characteristics. Also shown are model predictions at minimum and maximum mass. The pitching moment terms are the most important from a handling qualities perspective. Here, the agreement between model and flight is good, although the model overestimates the speed stability M_u with increasing airspeed. The primary pitch damping M_q and the angle of attack stability M_w are both modelled accurately, although the control sensitivity M_{η_s} is overestimated. **Figure 8** shows the terms in the rotor torque equation. This equation is unique to gyroplanes, or helicopters in autorotation and the helicopter literature indicates that no previous flight or theoretical estimates of these derivatives have ever been identified or calculated. Correlation between the model and flight is very good across the speed range. The speed damping term T_Ω is important, and it can be seen that it is accurately modelled .

The discrepancies in drag damping X_u and heave damping Z_w have proved impossible to resolve. The heave damping term Z_w in particular, is one derivative that intuitively and mathematically ought to be the most sensitive to modelling errors associated with simulation of the rotor wake. The effects of deploying a more sophisticated approach are been currently investigated.

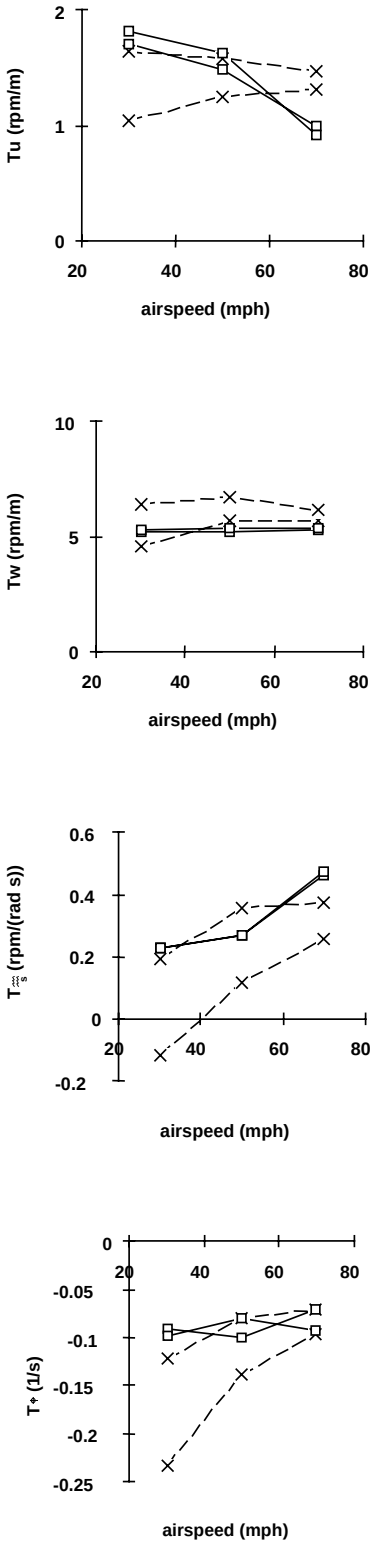

Figure 8: Rotor torque derivatives

Assessment of Gyroplane Longitudinal Flight Dynamics

The results derived from the extensive analysis of the VPM gyroplane data can be used to assess the stability performance of this gyroplane. Also, the validated blade element/individual blade model can be used to predict the performance of the Montgomerie gyroplane thus extending the assessment to the family of gyroplane aircraft.

VPM Stability Characteristics

The foregoing provides a qualitative and quantitative basis for the judgement that the identified models provide a good representation of the longitudinal flight dynamics of the VPM M16 gyroplane. It is argued that they can therefore be used to assess the nature of the type's stability and controllability characteristics.

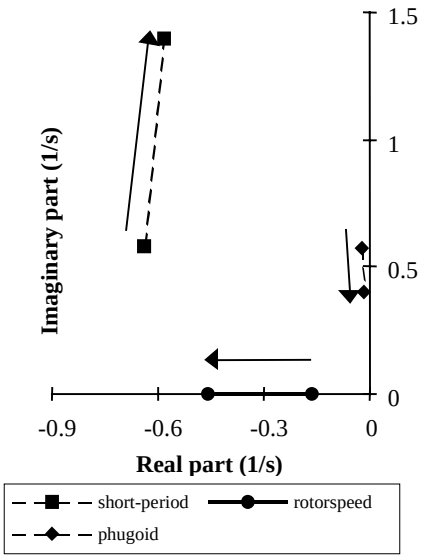

Figure 9: Identified model eigenvalues, 30, 70 mph

Figure 9 shows the eigenvalues of the synthesised models at 30 and 70 mph. The arrows indicate the progression from low to high speed. The two oscillatory modes are consistent with the frequency and damping of classical fixed-wing aircraft short-period and phugoid oscillations. The aperiodic mode is that of the rotorspeed degree of freedom. Assessment of the eigenvectors of the identified A matrices indicates that rotorspeed also features significantly in the rigid-body modes. The phugoid mode is relatively insensitive to changes in airspeed. The time to half amplitude is about 30-40 sec, its period 12-15 sec. The short-period mode is less than critically-damped throughout the speed range, with a damped natural frequency of between 0.1 and 0.25 Hz. The rotorspeed mode time to half amplitude lies between 1-4 sec.

A series of observations can be made by analysing the results illustrated in **Figure 7**. The relatively wide boundaries associated with X_u, and the small or even positive identified values are probably due to the fact that the propeller speed variations are not included in the model structure. The other derivative estimates all exhibit much narrower bounds. The aircraft exhibits "classical" static stability characteristics ($M_u > 0$, $M_w < 0$, $M_q < 0$) across the speed range. The derivative unique to the gyroplane is M_Ω, and being negative, will *tend* to be stabilising. This is because an increase in rotorspeed will result in a nose-down moment, tending to reduce the axial flow through the rotor, and hence tending to reduce the original rotorspeed disturbance.

The speed stability of the aircraft is indicated by M_u and the exhibited trend is consistent with the measured longitudinal stick position in trimmed flight. Unmodelled propeller speed and hence thrust variations may very well have a role to play in this derivative, quite apart from the usual rotor and tailplane contributions. The angle of attack stability M_w, unusually for a rotorcraft, is negative throughout the speed range. This is an important derivative as it holds the clue to a general understanding of gyroplane flight dynamics. Unaugmented rotorcraft generally rely on a horizontal tailplane to provide $M_w < 0$. This is because the natural tendency of the rotor (and hence thrust vector) is to flap back with angle of attack, or w disturbances. Since rotor thrust also increases with w, and the thrust line usually passes close to the centre-of-mass in undisturbed flight, then both effects sum to produce $M_w > 0$, Ref. 20. However, the profile of M_u and M_q with speed would tend to suggest that the tailplane on this gyroplane is somewhat ineffective, despite its relatively large size. This is consistent with wind tunnel tests on this configuration, Ref. 21. Pusher propeller configurations will tend to produce a

stabilising contribution to M_w as a consequence of the propeller normal force increasing with angle of attack disturbances. However, the relatively low power of the engine would suggest that this effect is small, and if considered with the very unclean aerodynamic environment in which the propeller operates, renders this phenomenon difficult to quantify.

Ref. 3 postulated that gyroplane longitudinal stability could be dominated by the vertical position of the centre-of-mass relative to the propeller thrust line, and a configuration with propeller thrust line below the centre-of-mass could exhibit $M_w < 0$ even at low airspeeds where any tailplane contribution would be negligible. The mechanism for this is shown in **Figure 10**.

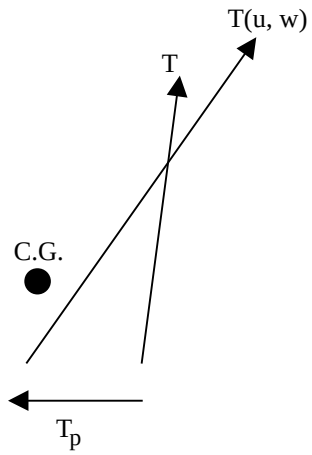

Figure 10: Rotor and Propeller Forces in Equilibrium and Disturbed Flight

The nose-up moment produced by a configuration with propeller thrust line below the centre-of-mass will require to be trimmed in equilibrium flight by having the main rotor thrust line passing behind the centre of mass as shown. In disturbed flight then, the possibility exists of the reduction in nose-down moment caused by the rotor flapping back, being overcome by the contribution from the increase in thrust, resulting in $M_w < 0$. Note that the result $M_\Omega < 0$ identified here is also consistent with such a configuration. Calculations based on mass and balance measurements do place the vertical position of the centre of mass 0.02 m above a line passing through the centre of the propeller hub.

Further validation of this postulate comes from the marked reduction in M_w (and M_Ω) at 50 mph. This is close to the minimum drag speed, and hence where the propeller thrust would be a minimum also. Any pitching moment from the propeller would therefore be a minimum, and the main rotor thrust line would be at its closest to the centre of mass in equilibrium flight, i.e. tending to give a smaller M_w than at the higher-power speeds of 30 and 70 mph.

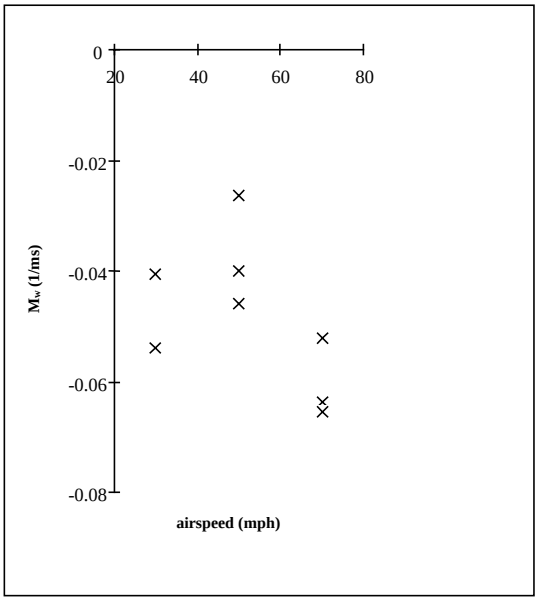

Figure 11: Multi-run consistency of result in M_w

Figure 11 shows estimates for M_w at each speed, obtained from different flights. The multi-run consistency exhibited serves to confirm $M_w < 0$ throughout the speed range, even at low speed, and also the observed effect that M_w is reduced in magnitude at around the minimum drag speed. **Figure 8** has illustrated the identified derivatives in the rotor torque equation. It is impossible to relate these to any previous quantitative work. However, qualitatively T_u and T_w are consistent with Glauert's seminal work, Ref. 4 in that an increase in airspeed and axial velocity will both tend to increase rotorspeed ($T_u > 0$, $T_w > 0$). Although the primary damping

term T_Ω decreases with airspeed, the rotorspeed mode itself exhibits the opposite trend. This indicates the extent of inter-modal coupling between the rotorspeed and body degrees of freedom. Finally, the control derivative T_{η_s} shows that the rotorspeed response will become increasingly sensitive to control application with airspeed.

Montgomerie Stability Characteristics

Given the good comparisons achieved in the validation exercise using the VPM data, it is possible to draw conclusions on the stability characteristics of other similar gyroplanes from simulation results. In the following sections the stability characteristics of the Montgomerie gyroplane are investigated.

Simulations were performed over a speed range of 30 mph to 75 mph in 5 mph increments. The trim aircraft attitudes are illustrated in **Figure 12**.

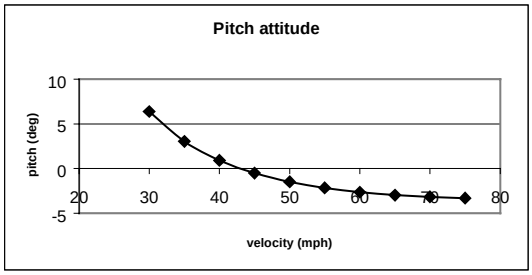

Figure 12a: Pitch trim angle for Montgomerie gyroplane

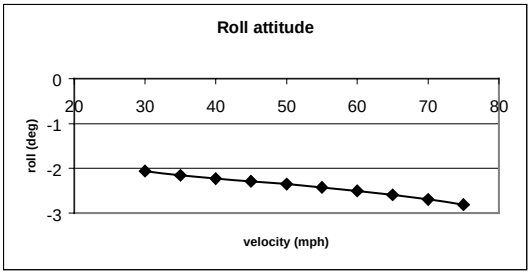

Figure 12b: Roll trim angle for Montgomerie gyroplane

The results are very similar to those for the VPM gyroplane, although the model predicts that this aircraft flies slightly more nose down. **Figure 13**, presents the control angles required, the trend again being similar to that of the VPM gyroplane.

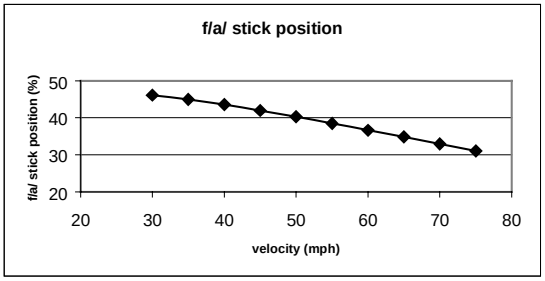

Figure 13a: Longitudinal trim stick for Montgomerie gyroplane

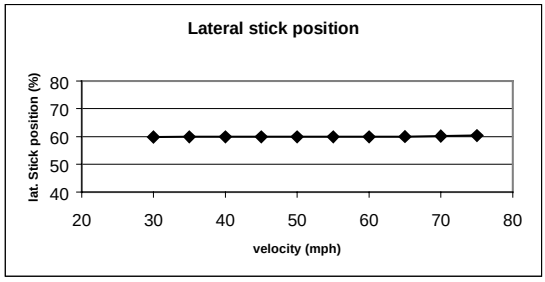

Figure 13b: Lateral trim stick for Montgomerie gyroplane

The rotorspeed predicted by the model is higher than that obtained for the VPM aircraft. This is consistent with fundamental gyroplane theory which states that rotorspeed is inversely proportional to the aircraft weight. The rotorspeed results are illustrated in **Figure 14**.

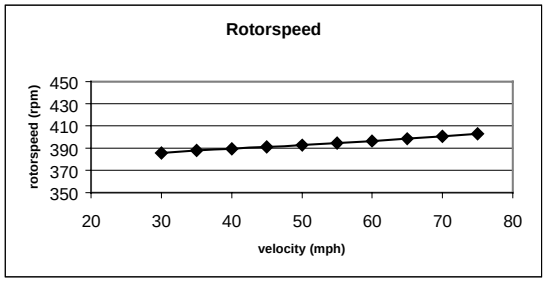

Figure 14: Rotorspeed for Montgomerie gyroplane

The preliminary studies of the longitudinal stability of the Montgomerie aircraft also suggest that it behaves similarly to the VPM gyroplane. The important result from the previous research regarding the effect of the vertical cg position with respect to the thrust line, was further validated using a parametric study on this aircraft. The effect of vertical cg position on M_w, which much influences longitudinal stability, is illustrated in **Table 2**.

c.g. position	M_w
10 cm above	-0.057
5 cm above	-0.050
nominal position	-0.042
5 cm below	-0.034
10 cm below	-0.027

Table 2: Variation of M_w with c.g. position

The results obtained from the initial simulations of the Montgomerie gyroplane, indicate that this aircraft possesses the same basic characteristics as the VPM gyroplane. The above findings will be enhanced and revisited where necessary, after the flight testing of the aircraft due to take place this summer.

Airworthiness and Flight Safety Issues

1. The results presented in this paper are unique in that the literature indicates that no previous in-flight investigation of gyroplane stability and control has taken place.
2. They have been produced for two different types of gyroplane and can be used to consolidate the understanding and document the attributes of this type of aircraft.
3. The results are timely in that the U.K. gyroplane accident record is poor, and a substantial number of fatal accidents remain largely unexplained. In addition, the U.K.'s new airworthiness and design standard BCAR Section T is a unique code, and requires substantive data, having been developed largely from other codes.
4. Contemporary flight test and data analysis techniques have been used, which helps to consolidate the status of system identification and parameter estimation for rotorcraft.

The gyroplane joins conventional single main and tail rotor helicopters, tandem rotor helicopters and tilt-rotors as rotorcraft that have enjoyed the successful application of these tools to a real engineering problem. As gyroplane stability and control has not featured in the literature until recently, documenting the characteristics of two different types benchmarks the quantification of gyroplane stability in general. Also, the result in M_w in particular, can be rationalised in terms of centre of mass position with respect to propeller thrust line, an issue of direct relevance to all gyroplanes. The results can also be applied directly to the development of the airworthiness and design standard BCAR Section T, as they constitute the only documentation of actual aircraft characteristics to date. For example, there is no requirement for balance to be specified in terms of vertical centre-of-mass position in relation to the propeller thrust line. The results suggest that this is an important consideration in conferring positive angle of attack stability M_w, which it is relatively easy to show has a key role to play in stabilising the phugoid mode of rotorcraft, Ref. 19.

Finally, the results quantify the extent to which the rotorspeed degree of freedom is significant in gyroplane flight mechanics. The pilot relies on management of flight state to maintain rotorspeed, having no direct control over it. Although the results indicate that the rotorspeed mode is stable, it is closely coupled with the conventional rigid body degrees of freedom. The rotor torque derivatives indicate that rotorspeed is sensitive to airspeed and angle of attack perturbations and this may have implications for handling in marginal situations.

Conclusions

Robust identification of gyroplane longitudinal stability and control derivatives has been possible using relatively straightforward frequency-domain parameter estimation tools.

Unusually for rotorcraft in general, the type examined displays "classical" longitudinal dynamic stability characteristics, and is stable throughout the speed range. However, rotorspeed is an important variable and is closely coupled with the conventional rigid-body degrees of freedom.

The Department's blade element/individual blade model has enjoyed one of the most comprehensive and in-depth comparisons with flight test data to be seen in the rotorcraft literature. It can now be used as a reliable tool in simulating

not only gyroplanes but helicopters in autorotational mode.

Interpretation of the identified stability derivatives indicates that the vertical position of the centre of mass in relation to the propeller thrust line may have an important role to play in gyroplane longitudinal stability.

The results from two different types of gyroplanes contribute directly to the development of the UK gyroplane airworthiness and design standard, BCAR Section T in the important areas of dynamic stability, and weight and balance.

Appendix

The following table presents the basic properties of the gyroplanes under investigation.

Parameter	VPM	Montgomerie
Mass (kg)	277.55	227.2
Ixx (kgm^2)	100	82
Iyy (kgm^2)	442	362
Izz (kgm^2)	556	456
No of blades	2	2
Blade radius (m)	4.15	3.81
Blade mass (kg)	18	13.15
Blade flapping inertia (kgm^2)	103.3	63.6
Blade aerofoil section	unknown	NACA 8H12
Blade chord (m)	0.218	0.197
Rotor direction (from above)	Anti-clockwise	Anti-clockwise
Propeller radius (m)	0.925	0.787
Propeller chord (m)	0.1	0.09
Xhub	(0.0969,0,-2.25)	(-0.038,0,-2.10)
Propeller hub location	(-0.68,0,-0.885)	(-0.950,0,-0.795)
Xcg	(0.014,0,-0.909)	(-0.08,0,-0.90)
Tailplane area (m^2)	0.9	0.356
Fin area (m^2)	0.19	0.281
Endplate area (m^2)	0.18	0.107
Rudder area (m^2)	0.34	0.368
Fuselage side area (m^2)	1.4	0.798
Fuselage plan area (m^2)	1.6	0.916
Fuselage front area (m^2)	0.59	0.448

Acknowledgement

Results presented for the VPM gyroplane were obtained as part of a study for the U.K. Civil Aviation Authority under Research Contract No. 7D/S/1125. The Technical Authority was Mr. David Howson.

References

1. Anon, "Airworthiness Review of Air Command Gyroplanes", Air Accidents Investigation Branch Report, Sept. 1991.

2. Anon, "British Civil Airworthiness Requirements, Section T, Light Gyroplane Design Requirements" Civil Aviation Authority Paper No. T 860 Issue 2, Jul. 1993.

3. Houston, S. S., "Longitudinal Stability of Gyroplanes", The Aeronautical Journal, Vol. 100, No.991, pp. 1-6, 1996.

4. Glauert, H., "A General Theory of the Autogyro", Aeronautical Research Committee Reports and Memoranda No. 1111, Nov. 1926.

5. Lock, C. N. H., "Further Development of Autogyro Theory Parts I and II", Aeronautical Research Committee Reports and Memoranda No. 1127, Mar. 1927.

6. Glauert, H., "Lift and Torque of an Autogyro on the Ground", Aeronautical Research Committee Reports and Memoranda No. 1131, Jul. 1927.

7. Lock, C. N. H., Townend, H. C. H., "Wind Tunnel Experiments on a Model Autogyro at Small Angles of Incidence", Aeronautical Research Committee Reports and Memoranda No. 1154, Mar. 1927.

8. Glauert, H., Lock, C. N. H., "A Summary of the Experimental and Theoretical Investigations of the Characteristics of an Autogyro", Aeronautical Research Committee Reports and Memoranda No. 1162, Apr. 1928.

9. Wheatley, J. B., "Wing Pressure Distribution and Rotor-Blade Motion of an Autogyro as Determined in Flight", NACA TR 475, 1933.

10. Wheatley, J. B., "An Aerodynamic Analysis of the Autogyro Rotor with a Comparison Between Calculated and Experimental Results", NACA TR 487, 1934.

11. Wheatley, J. B., Hood, M. J., "Full-Scale Wind-Tunnel Tests of a PCA-2 Autogyro Rotor", NACA TR 515, 1935.

12. Wheatley, J. B., "An Analytical and Experimental Study of the Effect of Periodic Blade Twist on the Thrust, Torque and Flapping Motion of an Autogyro Rotor", NACA TR 591, 1937.

13. Schad, J. L., "Small Autogyro Performance", Journal of the American Helicopter Society, Vol.10, No. 3, 1965, pp. 39-43.

14. McKillip, R. M., Chih, M. H., "Instrumented Blade Experiments Using a Light Autogyro", Proceedings of the 16th. European Rotorcraft Forum, Glasgow, Scotland, Sept. 1990.

15. Houston , S.S. “Validation of a non-linear individual blade rotorcraft flight dynamics model using a perturbation method,” The Aeronautical Journal, Vol. 98, (977), pp 260-266, Aug/Sept 1994.

16. Fu, K.-H., Marchand, M., "Helicopter System Identification in the Frequency Domain", Proceedings of the 9th. European Rotorcraft Forum, Stresa, Italy, Sept. 1983.

17. de Leeuw, J. H., "Identification Techniques, Model Structure and Time Domain Methods", AGARD LS178, pp. 5-1 to 5-9, October 1991.

18. Tischler, M. B., "Identification Techniques, Frequency Domain Methods", AGARD LS178, pp. 6-1 to 6-4, October 1991.

19. Padfield, G. D., "On the Use of Approximate Models in Helicopter Flight Mechanics", Vertica, Vol. 5, No. 3, 1981, pp. 243-259.

20. Bramwell, A. R. S., "Helicopter Dynamics", Arnold, London, 1976, pp. 199-200.

21. Coton, F., et. al., "Wind Tunnel Testing of a 1/3rd. Scale Model Gyroplane", Proceedings of the 9th. European Rotorcraft Forum, Sept. 1983.